

College of Saint Benedict and Saint John's University

DigitalCommons@CSB/SJU

---

Physics Faculty Publications

Physics

---

5-2012

## Ion acceleration in a helicon source due to the self-bias effect

Matt Wiebold

College of Saint Benedict/Saint John's University, [mwiebold@csbsju.edu](mailto:mwiebold@csbsju.edu)

Yung-Ta Sung

John E. Scharer

Follow this and additional works at: [https://digitalcommons.csbsju.edu/physics\\_pubs](https://digitalcommons.csbsju.edu/physics_pubs)



Part of the [Plasma and Beam Physics Commons](#)

---

### Recommended Citation

Weibold M, Sung YT, Scharer JE. 2012. Ion acceleration in a helicon source due to the self-bias effect. *Physics of Plasmas* 19(5): 053503.

This Article is brought to you for free and open access by DigitalCommons@CSB/SJU. It has been accepted for inclusion in Physics Faculty Publications by an authorized administrator of DigitalCommons@CSB/SJU. For more information, please contact [digitalcommons@csbsju.edu](mailto:digitalcommons@csbsju.edu).

## Ion acceleration in a helicon source due to the self-bias effect

Matt Wiebold, Yung-Ta Sung, and John E. Scharer

*University of Wisconsin-Madison, Electrical and Computer Engineering, Madison, Wisconsin 53706, USA*

(Received 15 December 2011; accepted 21 March 2012; published online 21 May 2012)

Time-averaged plasma potential differences up to 165 V over several hundred Debye lengths are observed in low pressure ( $p_n < 1$  mTorr) expanding argon plasmas in the Madison Helicon eXperiment (MadHeX). The potential gradient leads to ion acceleration greater than that predicted by ambipolar expansion, exceeding  $E_i \approx 7 kT_e$  in some cases. RF power up to 500 W at 13.56 MHz is supplied to a half-turn, double-helix antenna in the presence of a nozzle magnetic field, adjustable up to 1 kG. A retarding potential analyzer (RPA) measures the ion energy distribution function (IEDF) and a swept emissive probe measures the plasma potential. Single and double probes measure the electron density and temperature. Two distinct mode hops, the capacitive-inductive (E-H) and inductive-helicon (H-W) transitions, are identified by jumps in density as RF power is increased. In the capacitive (E) mode, large fluctuations of the plasma potential ( $V_{p-p} \gtrsim 140$  V,  $V_{p-p}/\bar{V}_p \approx 150\%$ ) exist at the RF frequency and its harmonics. The more mobile electrons can easily respond to RF-timescale gradients in the plasma potential whereas the inertially constrained ions cannot, leading to an initial flux imbalance and formation of a self-bias voltage between the source and expansion chambers. In the capacitive mode, the ion acceleration is not well described by an ambipolar relation, while in the inductive and helicon modes the ion acceleration more closely follows an ambipolar relation. The scaling of the potential gradient with the argon flow rate and RF power are investigated, with the largest potential gradients observed for the lowest flow rates in the capacitive mode. The magnitude of the self-bias voltage agrees with that predicted for RF self-bias at a wall. Rapid fluctuations in the plasma potential result in a time-dependent axial electron flux that acts to “neutralize” the accelerated ion population, resulting in a zero net time-averaged current through the acceleration region when an insulating upstream boundary condition is enforced. Grounding the upstream endplate increases the self-bias voltage compared to a floating endplate. © 2012 American Institute of Physics.

[<http://dx.doi.org/10.1063/1.4714605>]

### I. INTRODUCTION

Recent observation of double layers and accelerated ions in the expanding plume region of helicon sources has led to interest in their use as a source of thrust for spacecraft. Several researchers have observed the formation of current-free double layers (CFDLs) leading to ion acceleration<sup>1–11</sup> as well as ambipolar acceleration of ions in similar devices.<sup>12–16</sup> Charles<sup>17</sup> gives an excellent review of double layers, helicons, and their use as a thrust source.

Radio frequency (RF) plasma sources such as helicons often exhibit discontinuous mode hops or jumps as the coupling mechanism between the driving antenna and the plasma changes, a function of the skin depth for penetration of the RF fields into the plasma. If electron-neutral collisions are rare within an RF cycle ( $\nu_{en}^2 \ll \omega_{RF}^2$ , for argon at 13.56 MHz, this is satisfied for neutral pressures  $p_n \lesssim 25$  mTorr), the skin depth is given by<sup>18</sup>

$$\delta_p = \frac{1}{\alpha_p} = \sqrt{\frac{m_e}{e^2 \mu_0 n_e}}, \quad (1)$$

where  $\delta_p$  is the skin depth (meters),  $\alpha_p$  is the attenuation constant,  $m_e$  is the electron mass,  $n_e$  is the electron density, and  $\mu_0$  is the vacuum permeability. At the lowest electron densities, the imposed RF electric fields can easily penetrate the

plasma and directly heat the electrons, since the skin depth is much longer than the dimensions of the plasma, known as the capacitive coupling (E) mode. As ionization and electron density increase, the skin depth approaches the dimensions of the plasma, and the internal currents are induced to shield the imposed fields. This is known as the inductive (H) mode. In helicon reactors, antennas are designed to efficiently couple to helicon waves or modes in the magnetized plasma column. If the helicon wave dispersion relation (a function of the electron density, magnetic field and antenna  $\vec{k}$  spectrum) can be satisfied, the source can transition to the helicon (W) mode and a helicon wave can propagate, leading to the characteristic “blue mode” that is associated with helicon sources.

Accelerated ion populations are typically observed in helicon sources operated at low neutral pressures ( $p_n \lesssim 1$  mTorr) and moderate powers and magnetic fields that are characteristic of the capacitive or inductive modes. While some researchers have observed double layer formation in a “blue mode” helicon (see Cohen,<sup>10</sup> for example), it is possible some systems may not be operating in the helicon (W) mode when double layers or accelerated ions are observed. The mode of operation of the source, as will be shown, must be considered when interpreting these results.

In the presence of large-magnitude, rapid fluctuations of the plasma potential, which often occur in capacitively

coupled sources, the plasma electrons and ions may respond very differently to the rapidly fluctuating sheath fields near the plasma boundaries. An object immersed in a plasma floats to a potential that is a result of the balance between electron and ion flux to its surface. A sheath builds to retard the more mobile electrons and accelerate the ions to the surface. In an electropositive plasma, if the plasma potential is constant in time, the sheath potential is given by<sup>18</sup>

$$|V_{fl-DC}| = \frac{kT_e}{e} \ln \sqrt{\frac{M_i}{2\pi m_e}}, \quad (2)$$

where  $T_e$  is the (Maxwellian) electron temperature,  $M_i$  is the ion mass, and  $m_e$  is the electron mass. For argon, an object will float to a potential  $|V_{fl-DC}| = 5.2 kT_e/e$  below the plasma potential, which includes an additional  $0.5 kT_e/e$  drop through the presheath. In the presence of fluctuations in the plasma potential, the plasma electrons and ions may respond differently to time-dependent plasma potential gradients, depending on the relative time scales. Chabert<sup>19</sup> offers an explanation of the importance of the time scales by examining the motion of an ion in the presence of a sinusoidally varying electric field of the same order of magnitude of a sheath field:

$$\frac{d^2x}{dt^2} = \frac{e kT_e}{M e \lambda_D} \sin(\omega t), \quad (3)$$

where  $x$  is the ion position,  $M$  is the ion mass,  $T_e$  is the electron temperature,  $\lambda_D$  is the Debye length, and  $\omega$  is the driving frequency. The solutions to Eq. (3) will be of the form  $x(t) = -x_0 \sin(\omega t)$ ; therefore, the amplitude of the resulting oscillation amplitude will scale with driving frequency  $\omega$  as

$$\frac{x_0}{\lambda_D} = \frac{\omega_{pi}^2}{\omega^2}. \quad (4)$$

When the driving frequency  $\omega$  is greater than the ion plasma frequency  $\omega_{pi}$ , the oscillations of the ions will be smaller than a Debye length. A similar argument can be made for an electron in the same oscillating field, and the oscillations scale with the *electron* plasma frequency instead of the ion plasma frequency in Eq. (4). For the conditions examined here, the electron plasma frequency is much greater than the driving frequency ( $\omega_{pe}^2 \gg \omega_{RF}^2$ ), for example, at an electron density  $n_e = 10^9 \text{ cm}^{-3}$  and  $f_{RF} = 13.56 \text{ MHz}$ ,  $\omega_{pe}^2/\omega_{RF}^2 \approx 440$ . However, for our conditions, the ion plasma frequency is typically smaller than the driving frequency ( $\omega_{pi}^2 \lesssim \omega_{RF}^2$ ). For an ion density  $n_i = 10^9 \text{ cm}^{-3}$  and  $f_{RF} = 13.56 \text{ MHz}$ ,  $\omega_{pi}^2/\omega_{RF}^2 \approx 6 \times 10^{-3}$ . The result is a larger electron than ion flux (initially) to an object immersed in the plasma, and the time-averaged value of the sheath field increases to compensate, leading to a larger floating potential<sup>19,20</sup>

$$|V_{fl-RF}| = |V_{fl-DC}| + \frac{kT_e}{e} \ln \left[ I_0 \left( \frac{eV_1}{kT_e} \right) \right], \quad (5)$$

where  $V_{fl-DC}$  is given by Eq. (2) ( $|V_{fl-DC}| \approx 4.7 kT_e$  in argon),  $I_0$  is the modified Bessel function of the first kind,<sup>19,20</sup>

and  $V_1$  is the magnitude of the fluctuations. The increase in the time-averaged value of the floating potential in the presence of fluctuations in the plasma potential is known as the self-bias effect. RF plasma processing reactors can exploit the self-bias effect to control incident ion energies on substrates, which can be much greater than ion energies in DC sheaths.<sup>18</sup>

Dunaevsky<sup>16</sup> observed ion acceleration in a high-pressure capacitive capillary discharge, with ion energies exceeding 100 eV. A molybdenum gas feed, 0.6 mm wide and 18 mm long, acted as the positive electrode, and a ground electrode of copper foil was wrapped around the outside of the 1 mm wide and 10 mm long capillary. Argon gas was fed into the capillary at 2 to 10 sccm, resulting in pressures between 7 and 18 Torr. The discharge was driven with 2 MHz RF with antenna voltages between 210 V and 230 V, or an RF power of 15 to 20 W. Thrust on the order of 0.3 mN for 2 sccm of xenon was estimated and 0.4 mN at 10 sccm xenon with RF power below 20 W. No double layer structures were observed in the plume. This research gives experimental evidence that a capacitive discharge could be used to generate thrust. Though not discussed directly, the self-bias effect certainly plays a role in the observed ion acceleration.

Initial observation of accelerated ions in the Madison Helicon Experiment was detailed in an earlier publication,<sup>21</sup> where RF-timescale fluctuations in the plasma potential were not addressed. In order to discuss some of the aspects of the present work, a brief overview of the axial dependence of the ion energy reported previously is necessary. Retarding potential analyzer (RPA) measurements of the ion energy distribution function revealed a gradient in the “background” ion energy (assumed to be the plasma potential relative to ground) exceeding that predicted by ambipolar expansion theory, occurring over several hundred Debye lengths. The gradient in plasma potential led to the formation of an accelerated ion population that persisted for several ion-neutral charge exchange mean free paths. An electron density decrease by a factor of  $\approx 36$  was also measured through the acceleration region. The scaling of the potential gradient with magnetic field strength, argon flow rate and RF power were investigated, with ion energies exceeding  $E_i = 160 \text{ eV}$  measured at  $P_{RF} = 500 \text{ W}$  at low argon pressures (1.3 sccm argon flow rate,  $p_n \approx 10^{-4} \text{ Torr}$ ). The present work offers a deeper understanding of the observed ion acceleration in terms of the self-bias effect, with particular focus on the mode of operation of the source and RF-timescale fluctuations of the plasma potential.

Section II briefly describes the MadHeX experimental system. Section III describes the diagnostics used, including the retarding potential analyzer (RPA) and probes. Section IV presents the results, and Sec. V includes a discussion and interpretation of the results.

## II. EXPERIMENTAL APPARATUS

The Madison Helicon eXperiment (MadHeX) (Ref. 21) (shown in Fig. 1) is built around a 10 cm inner-diameter

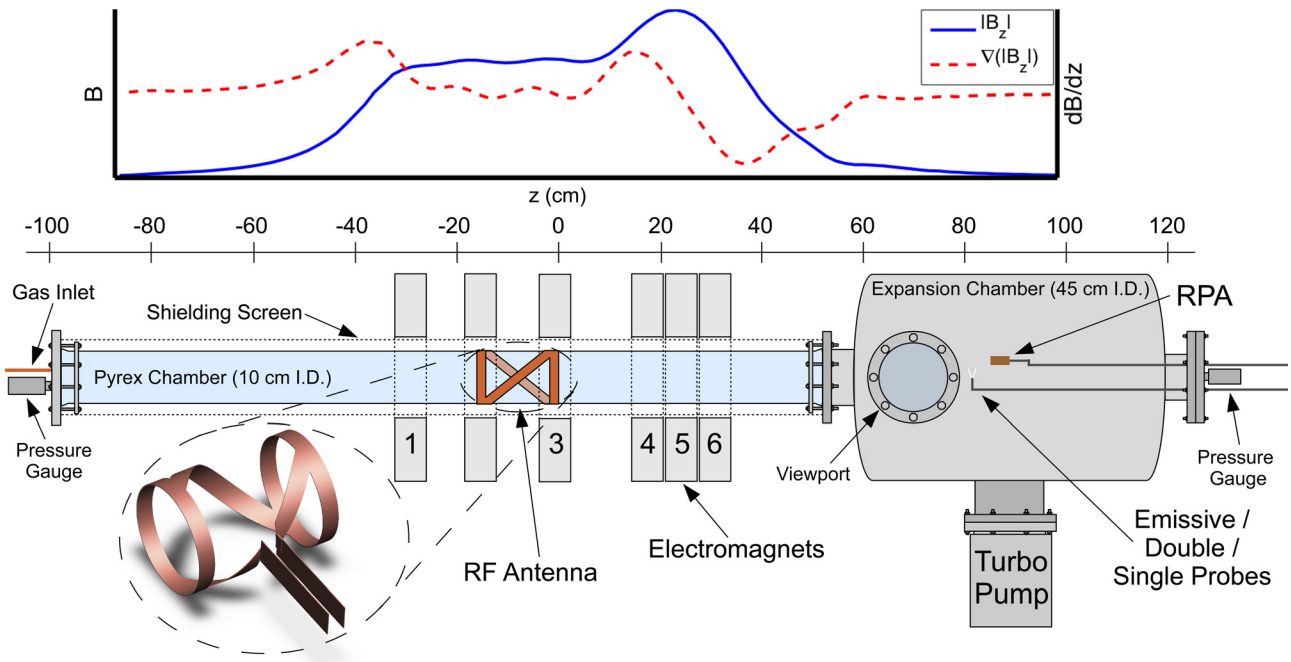


FIG. 1. Madison Helicon eXperiment (MadHeX). The RF antenna is shown in the lower left corner and the static magnetic field value and gradient are shown above the system.

(ID), 1.5 m long Pyrex chamber joined to a grounded, stainless steel expansion chamber, 45 cm in diameter and 70 cm long. Electrically grounded steel mesh (18 cm diameter) surrounds the Pyrex chamber. Argon gas flows into the Pyrex tube through a 5 mm I.D. copper tube through the left (upstream) aluminum endplate. An 8-in Varian turbomolecular pump is located at the bottom of the expansion chamber (downstream). MKS 910 DualTrans gauges located at the upstream and downstream endplates measure the pressure at these locations, and typical base pressures of the system are less than  $10^{-6}$  Torr. A half-turn, double-helix antenna, 18 cm long and 13 cm in diameter (pictured in the inset of Fig. 1) surrounds the Pyrex chamber. The downstream edge of the antenna denotes  $z=0$  cm in the system. Positive  $z$  is in the direction of the gas flow, from upstream to downstream.

The axial magnetic field is provided by six electromagnets, each 7 cm wide with an 18 cm bore. The magnetic field profile is configured in a “nozzle” profile with a mirror ratio  $R_m = 1.44$  with the peak at  $z = 28$  cm. A Sorensen DC power supply provides up to  $I = 180$  A, which corresponds to a magnetic field up to  $|B_z| = 1.04$  kG in the source region. Magnetic field values given below without a specified  $z$  position refer to the magnetic field value in the antenna region from  $z = 0$  to  $z = -18$  cm.

An RF signal at 13.56 MHz is provided by an HP 33120A function generator, which is then fed to a Comdel CX10KS amplifier, capable of delivering up to 10 kW steady-state. A two-capacitor matching network is used to match to the antenna impedance, and forward and reflected powers are measured with a Connecticut Microwave directional coupler with calibrated RF diodes. The matchbox is tuned to reduce the steady-state reflected power to below 5% of the incident power in steady-state for all cases shown.

### III. DIAGNOSTICS

#### A. Retarding potential analyzer

The retarding potential analyzer (RPA) used on the MadHeX system has been detailed in our previous publication.<sup>21</sup> It consists of a two grids, a floating entrance grid and a swept discriminator grid ( $V_d = 0$  to 300 V), and a biased ( $V_c = -9$  V) copper collector. The small physical size (12 mm diameter, 22 mm long) of the two-grid RPA reduces perturbation by the diagnostic compared to a larger, four-grid unit that was used to validate the two-grid unit.<sup>21</sup> The collector current is measured as a function of the discriminator bias and differentiated to extract the ion energy distribution function. The derivative of the collector current is actually related to the energy distribution of the ions falling through the sheath in front of the RPA but is often used in calculating the ion energy distribution function (IEDF).<sup>5</sup> In this work, the abbreviation “IEDF” refers to the differentiated collector current, which is proportional to  $v f(V_d)$ , where  $v$  is the ion velocity,  $V_d$  is the discriminator voltage, and  $f(V_d)$  is the ion energy distribution function.

The RPA measures the total ion energy, which is the sum of the ion potential energy (plasma potential) and the kinetic energy. In the absence of an accelerated (non-thermal) ion population, the RPA can be used to measure the plasma potential, or at least the kinetic energy gained by ions falling through the sheath in front of the analyzer. As discussed above in Sec. I, this results in a measurement of the *time-averaged* value of the sheath electric field (and plasma potential) if the plasma potential is rapidly fluctuating.

#### B. Emissive probe

The emissive probe used in MadHeX was also described in an earlier publication<sup>21</sup> but was used as a floating probe,

whereas in the present work, it is swept. The probe consists of a 25  $\mu\text{m}$  diameter, 6.8 mm long tungsten filament suspended between two ceramic-coated, gold-plated nickel wires. The filament is heated using a battery and simple resistor network, and the probe is biased relative to system ground using a custom probe supply based on the PA241 operational amplifier.

By sweeping the emissive probe filament bias with respect to chamber ground and measuring the collected current (similar to the operation of a single probe), the plasma potential can be measured using the inflection point method.<sup>22</sup> When the probe is not emitting (cold), it will act as a simple Langmuir probe. As filament current (and wire temperature  $T_w$ ) is increased, the inflection point (peak in the first derivative of the collected current with respect to the probe bias voltage) of the I-V trace will approach the plasma potential, assuming no RF modulation of the plasma potential is present. The plasma potential is calculated in the limit of zero emission by plotting the filament current versus the inflection point voltage. A straight line fit is used to extrapolate to zero emission current, which is interpreted as the plasma potential. This method has been shown to be accurate to within a few  $kT_e/e$  of the plasma potential.<sup>23</sup>

In the presence of plasma potential fluctuations, two or more peaks in the first derivative of the I-V trace may occur, depending on the number of significant harmonics present<sup>24,25</sup> and the time response of the probe system. Figure 2 illustrates the effect of a time-varying plasma potential on emissive probe analysis, for a probe whose time response is not fast enough to resolve the fluctuations, by modeling the probe current using

$$I(V_b) = I_0 \tanh[T(V_b - V_p)], \quad (6)$$

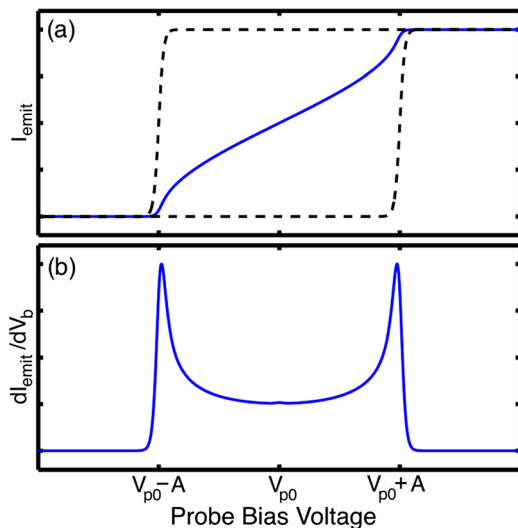


FIG. 2. Simulation of the effect of time-averaging on emissive probe analysis. (a) Time-averaged emitted current (blue, solid line) and instantaneous (black, dashed lines) emitted current vs probe bias voltage at the maxima of the plasma potential ( $V_p \pm A$ ) in the presence of a sinusoidal modulation of the plasma potential ( $V_p(t) = V_{p0} + A \sin[\omega_{RF}t]$ ). (b) The derivative of the time-averaged emitted current with respect to the bias voltage, showing two peaks at the maxima of the plasma potential modulation. Time-averaging is done over many RF cycles.

where  $I_0$  and  $T$  are scaling constants,  $V_b$  is the probe bias, and  $V_p$  is the plasma potential. In the absence of time-variation of the plasma potential [ $V_p \neq V_p(t)$ ], the emitted electron current from the heated probe is ideally zero when the probe bias is above the plasma potential and non-zero when the probe bias is below the plasma potential. The finite temperature of the filament and emitted electrons leads to a thermally broadened onset of emission as modeled by Eq. (6). In the presence of time-variation of the plasma potential, the instantaneous collected current as a function of bias voltage will oscillate in time. The black dashed lines in Fig. 2(a) denote the maximum excursions of the probe current, a result of a modulation of the plasma potential with the form  $V_p(t) = V_{p0} + A \sin[\omega_{RF}t]$ . At a constant probe bias voltage, if the probe and associated electronics are able to respond on the timescale of the fluctuations, the probe will “follow” these fluctuations and collect a time-varying current from which the plasma potential as a function of time could be calculated. However, if the probe is unable to follow the fluctuations due to stray or inherent impedances of the probe and electronics, the probe will collect (or emit) a *time-averaged* current. In Fig. 2(a), the blue solid line indicates the time-averaged value of the emitted current. Two peaks appear in the derivative of the probe current as shown in Fig. 2(b), and the bias voltages of the inflection points (peaks) approach the maximum excursions of the plasma potential.

The first derivative curve can also be interpreted as a “binning” or histogram of the values of the plasma potential averaged over many RF cycles, showing the relative amount of time spent at each value. For a purely sinusoidal modulation, the peaks in the histogram are symmetric about the unweighted mean of the peak locations and are of the same magnitude (see Fig. 2(b)), and the time-averaged value is the unweighted mean. If the modulation is asymmetric, the time-averaged value is the *weighted* mean of the histogram. As will be shown below, in our system, there are asymmetric inflection points in the emissive I-V curve, representing asymmetric RF plasma potential fluctuations, but the time-averaged plasma potential can be calculated from the first derivative of the emissive I-V curves using a weighted mean.

### C. Single and double probes

A combination planar single and double probe is used in MadHeX to measure the electron density and temperature. While also described in an earlier publication,<sup>21</sup> the analysis method used to extract the electron temperature  $T_e$  has been improved. As will be shown below, significant fluctuations in the plasma potential on the RF timescale are present, which can lead to difficulty in extracting an electron temperature from probe data. Typically, compensated probes can mitigate these effects if the fluctuations are small enough,<sup>26,27</sup> but the magnitude of the fluctuations observed in the capacitive coupling mode, exceeding  $V_{p-p}/\bar{V}_p \approx 150\%$  in the present case, make compensation impractical. It should be noted that densities are measured with the probes biased in ion saturation (large, negative bias); therefore, ion density is measured, which is assumed equal to the *time-averaged* electron density. The electrons, able to respond to rapidly oscillating

gradients in the plasma potential, may have a rapidly varying local density, which these probes are not built to measure.

Oksuz<sup>28</sup> suggested that despite the presence of large-magnitude fluctuations of the plasma potential, an electron temperature can be extracted from a single probe I-V trace if the EEDF is assumed to be Maxwellian. The collected electron current is affected by the rapidly oscillating plasma potential relative to the probe bias, which is nearly constant on the RF timescale (3 Hz sweep frequency). An uncompensated probe, unable to “follow” the rapid fluctuations in the plasma potential, collects a time-averaged current as a function of the probe bias voltage, leading to erroneous measurement of the electron temperature if the fitting or analysis is performed in a part of the I-V curve affected by the fluctuations in the plasma potential. If the probe bias voltage is inside the “window” formed by the upper and lower limits of the plasma potential fluctuations, the probe collects a time-averaged current and an electron temperature cannot be reliably extracted. If the probe bias voltage is outside of the plasma potential fluctuation window, the probe will still collect a time-averaged current but now represents the “edge” or “tail” of the electron distribution when the instantaneous oscillating plasma potential is at its minimum.

The swept emissive probe described above allows a measurement of the fluctuation window and verification that the electron temperature fit is outside of the fluctuation window. However, the fitting only reveals the temperature of the electrons in the “tail” of the distribution, and no direct measurement of the full EEDF is possible. Improvements in the analysis of single probe data following the above technique has led to a correction to Fig. 7 in our earlier work,<sup>21</sup> the corrected version of which is shown below in Fig. 6 and discussed in Sec. V.

## IV. RESULTS

### A. Antenna coupling modes

Operation of our helicon source has revealed several operating modes as detailed above, a phenomenon commonly seen in similar sources (see Perry<sup>29</sup> or Ellingboe,<sup>30</sup> for example). Measurements of the electron density show a marked jump as RF input power is increased, as shown in Fig. 3 for an argon flow rate ( $Q$ ) of 2 sccm ( $p_n = 0.53$  mTorr at the upstream endplate,  $p_n = 0.16$  mTorr at the downstream endplate) and magnetic field of 340 G in the source region. The double probe measures  $n_e$  at  $z = 50$  cm as RF power is increased from 80 W to 300 W. Between  $P_{RF} = 200$  W and  $P_{RF} = 220$  W, there is an increase in the electron density from  $7 \times 10^9 \text{ cm}^{-3}$  to  $1.5 \times 10^{10} \text{ cm}^{-3}$ , indicating a capacitive to inductive mode transition. In Fig. 3, error bars shown are the standard deviation of the set of four measurements: the up-sweep and down-sweep for positive probe bias and negative probe bias ion saturation current (electron density) measurements.

There are several indicators that this particular density jump is evidence of the E-H transition and not the inductive to helicon (H-W) transition. First, if this was the H-W transition, there would likely be a distinct blue core in the plasma after the transition, a feature of “true” helicon wave mode

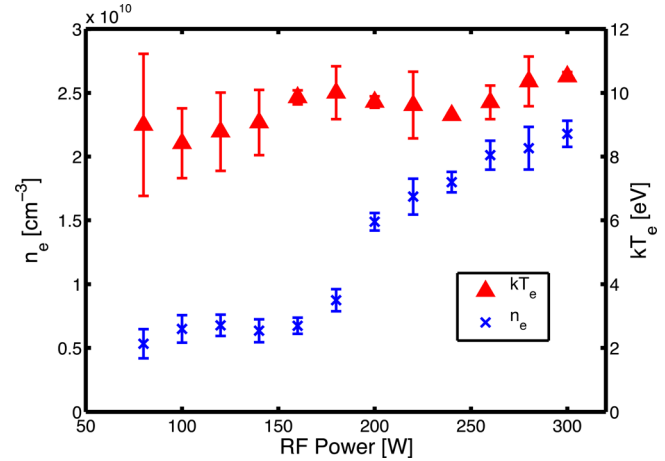


FIG. 3. Electron density (blue  $\times$ s, left axis) and electron temperature (red triangles, right axis) measured with the double probe for  $B = 340$  G,  $Q = 2$  sccm, and  $z = 50$  cm as a function of RF power. Error bars denote the standard deviation of a set of four measurements for the density and two for the electron temperature.

coupling. Second, as will be shown below, there are significant RF-timescale fluctuations of the plasma potential before the transition (see below), a feature of capacitive coupling, which are greatly reduced (by a factor of  $\sim 5$ ) after the transition. Lastly, the plasma densities before and after the transition (a few  $10^9 \text{ cm}^{-3}$  to  $10^{10} \text{ cm}^{-3}$ ) are characteristic of the capacitive and inductive mode and are much too low to be in the helicon mode. The H-W transition has also been observed, with the majority of earlier work on this experiment (Tysk<sup>31</sup> and Denning,<sup>32</sup> for example) focusing on wave effects and neutral depletion in the helicon mode. While of interest, the H-W transition will not be explored in the present work, as the observed self-bias effect and ion acceleration are most pronounced when RF-timescale fluctuations of the plasma potential are largest, which occurs in the capacitive (E) mode. Ion acceleration does occur in the H and W modes but can be explained by an approximation of ambipolar plasma expansion and does not exhibit a substantial self-bias effect for the cases examined.

Our earlier observation of large potential differences ( $\Delta V > 100$  V) exceeding that predicted by ambipolar expansion<sup>21</sup> led to further investigation of the operation of the source and the scaling of the potential gradient, including RF power scaling studies investigating the distinct mode jumps observed. The RPA was used to measure the difference in ion energy (see discussion below in Sec. V B) between the source and expansion chambers and subsequent accelerated-ion energy across the E-H mode transition as RF power was increased, which is shown in Fig. 4. As discussed above in Sec. III A, the RPA measures the kinetic energy of ions falling through the sheath in front of the analyzer, which is the time-averaged value of the plasma potential ( $V_p = E_i/e$ ) if the plasma potential is rapidly fluctuating. The plasma potential drop  $\Delta V$  is calculated from the difference between the upstream plasma potential (at  $z = 50$  cm) and the downstream plasma potential (at  $z = 90$  cm). Figure 5 delineates the upstream and downstream regions, as well as the physical location of the accelerated ion population. Also shown in

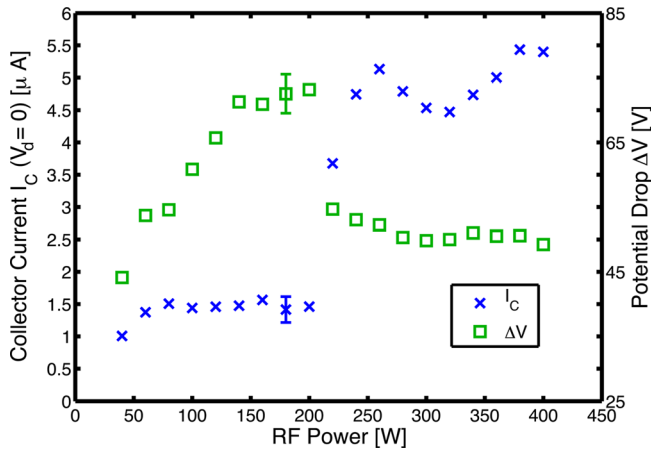


FIG. 4. RPA collector current at discriminator voltage  $V_d=0$  (left, blue  $\times$  s) and potential difference  $\Delta V$  (right, green open squares) vs RF power across the E-H transition for  $Q=2$  sccm,  $B=340$  G. The potential difference  $\Delta V$  is calculated from the upstream ( $z=50$  cm) and downstream ( $z=90$  cm) time-averaged plasma potentials, and the collector current  $I_c$  is measured at  $z=50$  cm.

Fig. 4 is the collector current at a discriminator voltage  $V_d=0$ , indicative of the ion density, at  $z=50$  cm. There is a distinct jump in the potential difference  $\Delta V$  between the source and expansion chambers across the E-H mode transition, from  $\Delta V=72 \pm 2$  V at  $P_{RF}=200$  W to  $\Delta V=54 \pm 2$  V at  $P_{RF}=220$  W. In the E mode ( $P_{RF} < 200$  W), the potential difference increases with RF power, from  $\Delta V=45 \pm 2$  V at  $P_{RF}=40$  W to  $\Delta V=72 \pm 2$  V at  $P_{RF}=200$  W, right before the mode transition. In the H mode, the potential difference magnitude varies much less, with a slight decrease of about 5 V from  $P_{RF}=220$  W to  $P_{RF}=400$  W. The uncertainty in the RPA ion energy measurements arises from the fitting used to approximate the peak in the ion distribution.

## B. Electron density and temperature

The electron density and electron temperature are shown in Fig. 6 for  $z=50$  cm to  $z=80$  cm for  $Q=2$  sccm,  $P_{RF}=100$  W, and  $B=340$  G. Note that the method used to extract an electron temperature is improved compared to that used previously,<sup>21</sup> resulting in an increase (compared to the previous measurement method) of  $\approx 2.5$  eV in the region upstream of  $z < 56$  cm and no significant change downstream of  $z > 56$  cm. The ion (and electron) density, measured with the single (Langmuir) probe biased in ion saturation (large negative bias), decreases rapidly through the ion acceleration region ( $z=50$  cm to  $z=65$  cm) from  $8.8 \times 10^9$  cm<sup>-3</sup> to  $2.4 \times 10^8$  cm<sup>-3</sup> (a factor of  $\approx 36$ ) from

$z=50$  cm to  $z=65$  cm, and then rises slowly to  $7 \times 10^8$  cm<sup>-3</sup> from  $z=65$  cm to  $z=80$  cm. The electron temperature  $kT_e$  from the single probe remains between 8.5 and 9.5 eV throughout the acceleration region, with no statistically significant change. The electron temperature fit has been carried out at probe bias voltages below the minimum in the plasma potential fluctuations to reduce the effects of the fluctuations (see above discussion).

## C. Plasma potential fluctuations

The abrupt decrease in the time-averaged plasma potential difference  $\Delta V$  across the E-H transition (shown in Fig. 4) led to further investigation of the source operation in the capacitive mode. The swept emissive probe revealed significant fluctuations in the plasma potential on the RF timescale, a key component in the development of the self-bias effect.

The swept emissive probe was used at  $z=50$  cm for the same conditions that produced an accelerated ion population with  $E_i=65$  eV in our previous work<sup>21</sup> ( $Q=2$  sccm,  $B=340$  G, and  $P_{RF}=100$  W), where the source is operating in the capacitive mode. Figure 7 shows the collected current (blue, solid line) and the derivative of the current with respect to bias voltage (green, dashed line). The collected current as a function of bias voltage is time-averaged, a result of the probe's inability to fully follow the rapid fluctuations. The black, vertical dashed lines indicate the ion energy measured with the RPA and the time-average of the plasma potential fluctuations, calculated from the weighted mean of the first derivative of the collected current. As discussed in Sec. III B, the derivative is in effect a histogram of the relative amount of time the plasma potential spends at each value; therefore, the weighted average of the histogram is equivalent to the time-averaged value of the plasma potential. The data in Fig. 7 show that at  $z=50$  cm, the plasma potential fluctuates between  $V_{p-min} \approx 5$  V and  $V_{p-max} \approx 145$  V, with a time-averaged value  $\bar{V}_p \approx 100$  V. The RPA, for the same conditions and axial location, measures a time-averaged plasma potential (ion energy) of  $E_i=100 \pm 3$  eV, evidence that the ions remain near the time-averaged value of the plasma potential.

The plasma potential modulation window (maximum and minimum values) and the time averaged value are shown as a function of  $z$  in Fig. 8 for the same conditions in Fig. 7 ( $Q=2$  sccm,  $B=340$  G, and  $P_{RF}=100$  W). The potential energy of the ions (the time-averaged value of the plasma potential), measured with the RPA, is also shown as black  $\times$  s. It is interesting to note that due to the strong fluctuations of the plasma potential, there will be a part of the

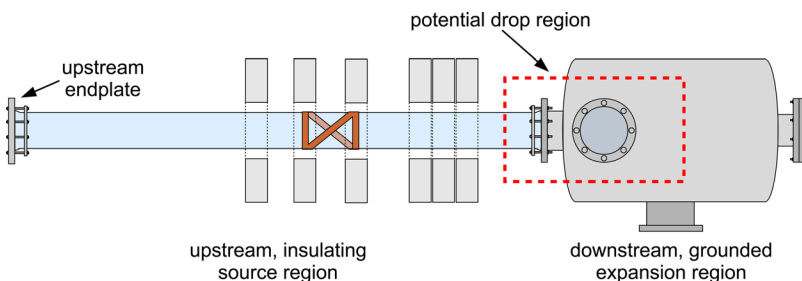


FIG. 5. System diagram for reference during discussion of results. The upstream and downstream regions are shown, as well as the region of the observed potential drops (red dashed box). The upstream endplate is also noted, which can be floated or grounded.

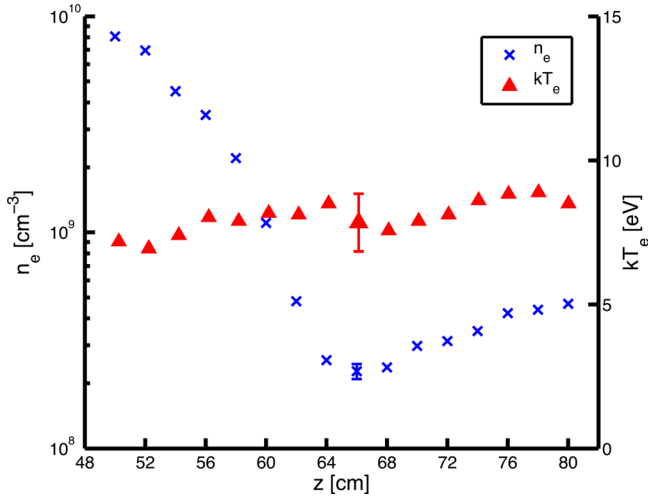


FIG. 6. Electron density (blue  $\times$ s) and temperature (red triangles) measured with the single probe for  $z=50$  cm to  $z=80$  cm for  $Q=2$  sccm,  $P_{RF}=100$  W, and  $B=340$  G.

RF cycle when the instantaneous plasma potential gradient is much smaller than the time-averaged plasma potential gradient. The electrons, which are able to fully respond to the instantaneous plasma potential profile, can easily transit the “acceleration region” between the upstream and downstream regions during an RF cycle. On a time-average basis, these electrons “neutralize” any ion beam that forms due to the time-averaged plasma potential gradient. The ions, however, cannot respond as quickly and feel the effects of the *time-averaged* plasma potential gradient. The differing response of the electrons and ions is the basis of the self-bias effect, discussed further below.

## V. DISCUSSION

### A. Boltzmann plasma expansion

Ambipolar (Boltzmann) plasma expansion is characterized by the balance between the gradient in the electron pressure ( $p_e = n_e kT_e$ ) and an ambipolar electric field that forms

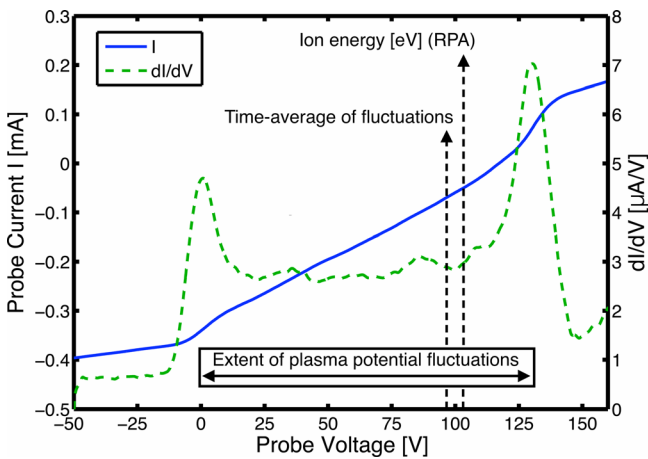


FIG. 7. Emissive probe I-V trace (blue, solid line) and first derivative (green, dashed line) at  $z=50$  cm for  $P=100$  W,  $Q=2$  sccm, and  $B=340$  G. The vertical arrows indicate the time-averaged value of the plasma potential and the ion energy (in eV) measured with the RPA. The horizontal arrow indicates the extent of the plasma potential fluctuations.

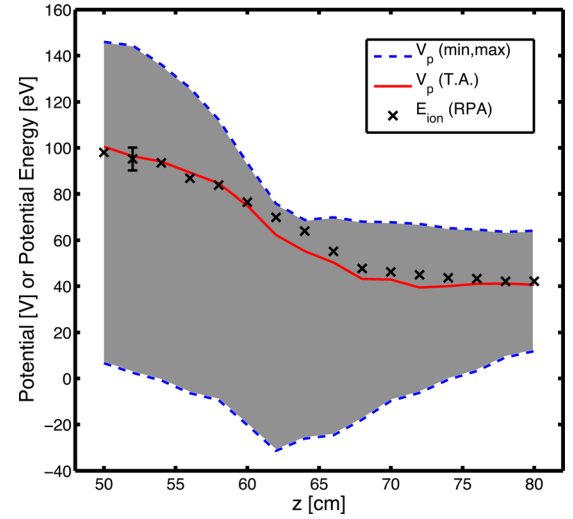


FIG. 8. Upper and lower limits (blue dashed lines) and time-averaged value (red solid line) of the plasma potential as measured with the swept emissive probe for  $Q=2$  sccm,  $P_{RF}=100$  W, and  $B=340$  G. Also shown is the ion potential energy as measured with the RPA (black  $\times$ s).

to retard electrons and accelerate ions to maintain neutrality.<sup>18</sup> The plasma potential and electron density are related through the Boltzmann relation

$$n_e(z) = n_{e0} \exp \left[ \frac{e(V_p(z) - V_{p0})}{kT_e} \right], \quad (7)$$

where  $V_p(z)$  is the local plasma potential,  $V_{p0}$  is the plasma potential at  $z=0$ ,  $n_e(z)$  is the local electron density,  $n_{e0}$  is the electron density at  $z=0$ , and  $T_e$  is the (Maxwellian) electron temperature. Equation (7) can be solved for the potential profile as a function of the electron density  $n_e(z)$

$$V_p(z) = V_{p0} + \frac{kT_e}{e} \ln \left[ \frac{n_e(z)}{n_{e0}} \right]. \quad (8)$$

If the electron density  $n_e(z)/n_{e0}$  is plotted versus the potential  $V_p(z) - V_{p0}$ , the electron temperature can be determined from a fit to the resulting curve. For a given set of experimental conditions, if the fitted (Maxwellian) electron temperature from the density and plasma potential data matches the measured electron temperature, it is assumed that the expansion is following the Boltzmann relation (see West,<sup>33</sup> for example).

A least-squares fit to Eq. (7) was performed on the spatial variation of the electron density (from the double probe) for  $P_{RF}=100$  W as a function of time-averaged plasma potential (RPA, see Sec. IV C), plotted on a semi-log scale, the result of which is shown in Fig. 9. The calculated electron temperature  $kT_e = 15.5 \pm 1.5$  eV is substantially higher than that measured with the single probe of  $kT_e = 9.0 \pm 1.1$  eV at  $z=50$  cm, an indication that the expansion is not well described by an ambipolar relation. Of course, the significant plasma potential fluctuations measured in the capacitive mode (shown in Fig. 8) suggest the electrons and ions will respond differently, so it should not be expected that simple ambipolar expansion applies to these conditions. The electrons, which can respond to the rapid fluctuations in the

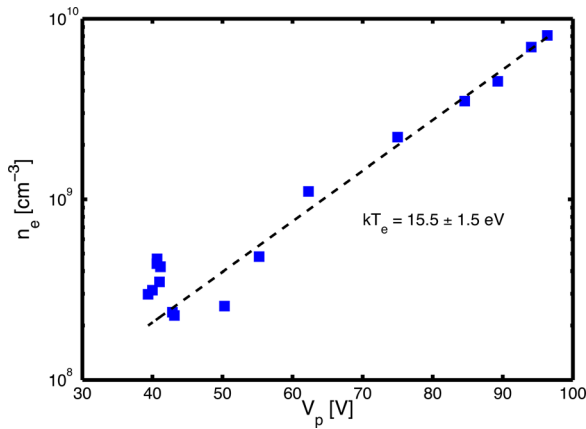


FIG. 9. Time-averaged electron density (single probe) plotted versus ion (potential) energy from the RPA for  $Q = 2$  sccm,  $P = 100$  W, and  $B = 340$  G. A least-squares fit to Eq. (7), calculated on a linear scale, is also shown (black dashed line) as well as the resulting Maxwellian electron temperature from the fit.

plasma potential profile, obey a Boltzmann relation in response to the time-dependent plasma potential profile, but the time-dependent electron density is very difficult to measure experimentally. The ions, which respond only to the time-averaged plasma potential, do not follow a Boltzmann relation.

For the same conditions, as the RF power is increased past  $P_{RF} \approx 200$  W the source transitions to the inductive mode. Here, the expansion more closely follows an ambipolar relation, as shown in Fig. 10. The required electron temperature to satisfy a Boltzmann expansion for this case is  $kT_e = 11.5 \pm 2$  eV, quite close to the measured value of  $kT_e = 11.0 \pm 0.8$  eV with the double probe.

## B. Self-bias effect

It is of interest to determine the reason the potential differences exceed that predicted by ambipolar or Boltzmann plasma expansion when the source is operating in the capacitive mode. The large RF fluctuations of the plasma potential observed in the capacitive mode offer insight into the mecha-

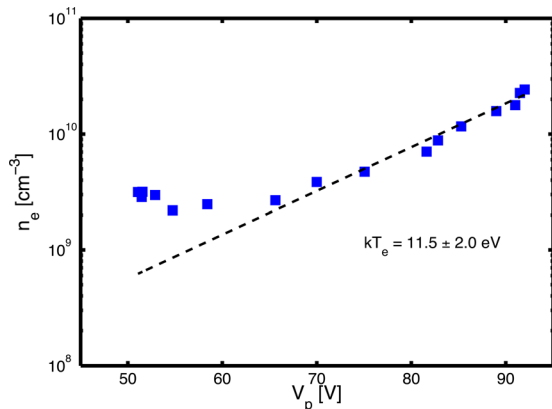


FIG. 10. Time-averaged electron density (single probe) plotted versus ion (potential) energy from the RPA for  $Q = 2$  sccm,  $P = 500$  W and  $B = 340$  G. A least-squares fit to Eq. (7), calculated on a linear scale, is also shown (black dashed line) as well as the resulting Maxwellian electron temperature from the fit.

nism; the upstream plasma is “self-biasing” to a higher time-averaged plasma potential relative to the plasma potential in the grounded expansion chamber.

The electron plasma frequency  $\omega_{pe}$  is significantly larger than the RF frequency for densities characteristic of the capacitive (E) mode. For instance, the electron density at  $z = 50$  cm for  $Q = 2$  sccm,  $B = 340$  G, and  $P_{RF} = 100$  W is  $n_e = 8.8 \times 10^9$  cm $^{-3}$ ; therefore,  $\omega_{pe}^2/\omega_{RF}^2 \approx 3800$ . The electrons are easily able to transit the scale length of the acceleration region and possibly the length of the system in an RF period. On the other hand, the ion plasma frequency is only  $\omega_{pi}^2/\omega_{RF}^2 \approx 5\%$  of the RF frequency for the same density, and the ions are unable to respond to the rapid changes in the plasma potential and its gradient in an RF cycle. Instead, the ions respond to the time-averaged plasma potential profile as indicated in Fig. 8. The electrons can readily flow from the upstream region during an RF cycle, whereas the ions cannot, and there is an initial imbalance of flux. This imbalance is short-lived, as the steady state fluxes of electrons and ions must balance over an RF cycle (assuming no net current flow). A time-averaged (DC) potential difference builds to retard electron flux and increase ion flux, and this increase is the self-bias voltage described in Eq. (5). For a higher electron density of  $1.6 \times 10^{11}$  cm $^{-3}$ ,  $\omega_{pi} = \omega_{RF}$ , and the ions will be better able to follow the fluctuations. However, at these densities, the source is operating in a mode where the plasma potential fluctuations are much reduced, either the inductive or the helicon mode. The higher electron density allows the plasma to better shield the RF antenna electrostatic fields as the skin depth  $\delta_p = c/\omega_{pe}$  decreases, for instance,  $\delta_p \approx 1.3$  cm for low collisionality ( $\nu_{en} \ll \omega_{RF}$ ) at  $n_e = 1.6 \times 10^{11}$  cm $^{-3}$ . When the ion density is high enough such that they can follow the fluctuations, the fluctuation magnitude is reduced in the source.

In the case of ambipolar expansion, the ambipolar (retarding) electric field increases until enough electrons are confined such that the ion and electron fluxes are equal from the source region. The electron diffusion over the ambipolar potential gradient is directly related to the number of electrons in the distribution with sufficient energy to overcome the ambipolar field, which can be calculated from the electron temperature in a Maxwellian electron distribution. Therefore, the ambipolar electric field and potential profile are a function of the electron temperature. However, in the present case, the plasma potential gradient between the two chambers is fluctuating due to the capacitive coupling of the antenna to the plasma, and the resulting electric field that forms is not necessarily dictated strictly by the electron temperature or distribution. The field instead adjusts such that electron and ion fluxes through the potential gradient are equal. The electron temperature still plays a role in the system equilibrium and the self-bias effect (see Eq. (5)), but the potential difference between the source and expansion regions is not necessarily limited by the ambipolar potential, set by the density gradient and electron temperature. The resulting potential gradient and electric field are a result of the self-bias effect.

In the present case, the time-averaged plasma potential in the expansion chamber is held at roughly the DC floating

potential ( $5kT_e/e \sim 40 - 50\text{V}$ ) by the grounded walls (see Sec. I). The upstream plasma, inside an insulating chamber (radial boundary condition is glass, end boundary condition discussed below), is able to charge relative to the downstream plasma. The insulating glass walls do not provide an “anchor” for the plasma potential in the source region, since they are allowed to float. However, the transition region between the source and expansion chambers, which would normally support a potential gradient set by simple ambipolar expansion, supports a much larger potential difference due to the increased axial electron flux from the source region due to the RF timescale plasma potential fluctuations. Of course, the situation is always self-consistent, such that the global electron and ion losses from the plasma are equal in steady state (no net current drawn from the plasma as a whole). The upstream boundary condition, explored below in Sec. V C, affects the distribution of the losses in the system and the restriction on current flow through the source region. In the case of the floating upstream endplate, the plasma in the upstream source region self-biases relative to the downstream plasma in the expansion chamber such that the time-averaged electron and ion fluxes from the upstream source to the downstream chamber are equal. When the upstream endplate is grounded, the same occurs, except equality of the *net* electron and ion fluxes from the upstream region (to the endplate as well as to the downstream chamber) is satisfied. Typically, a large plasma potential gradient would allow only the most energetic electrons to reach the downstream chamber. However, the rapid, time-dependent plasma potential fluctuations allow a sufficient number of electrons to transit the acceleration region during some part of the RF cycle and large time-averaged plasma potential differences can be supported without a net time-averaged current flow, if such a condition is enforced by the boundaries.

It is possible to estimate the magnitude of the expected self-bias voltage using Eq. (5), where the additional self-bias voltage due to the plasma potential fluctuations is given by

$$V_{SB} = |V_{fl-RF}| - |V_{fl-DC}| = \frac{kT_e}{e} \ln \left[ I_0 \left( \frac{eV_1}{kT_e} \right) \right], \quad (9)$$

where  $V_{SB}$  is the increase in the floating potential due to the plasma potential fluctuations,  $V_1$  is the amplitude of the fluctuations, and  $T_e$  is the electron temperature. From Fig. 8, the amplitude of the fluctuations at  $z = 50\text{ cm}$  is  $V_1 \approx 70\text{ V}$  for  $Q = 2\text{ sccm}$ ,  $P = 100\text{ W}$ , and  $B = 340\text{ G}$ . The electron temperature  $kT_e \approx 9\text{ eV}$  for these conditions (measured with the single probe); therefore, the predicted self-bias voltage is  $V_{SB} \approx 53\text{ V}$ . The measured potential difference from  $z = 50\text{ cm}$  to  $z = 80\text{ cm}$  for the same conditions is  $\Delta V \approx 65\text{ V}$ , higher than that predicted. However, the fact that the time-averaged value of the plasma potential fluctuations is not equal to the midpoint between the maximum and minimum plasma potential is evidence that the plasma potential fluctuations contain multiple harmonics of the fundamental RF frequency. As discussed by Chabert,<sup>19</sup> additional harmonics increase the self-bias voltage, with each harmonic contributing an extra factor  $\ln[I_0(a_i)]$  where  $a_i$  is the contribution of the  $i$ th harmonic, if the harmonics are in phase.

### C. Upstream boundary condition

The presence of the grounded upstream endplate allows for the possibility of net current flow through the system that can result in a potential gradient that is larger than that predicted by ambipolar plasma expansion. In order to show that a net current flow is not responsible for the larger-than-ambipolar plasma potential gradients, the upstream endplate was electrically insulated (floated) from system ground. The flow rate dependence of the potential difference (between  $z = 50\text{ cm}$  and  $z = 90\text{ cm}$ ) for both a grounded upstream endplate (green, open squares) and a floating upstream endplate (blue  $\times$ s) for  $B = 340\text{ G}$  and  $P_{RF} = 100\text{ W}$  is shown in Fig. 11. A potential difference still exists when the upstream endplate is floated, but the overall magnitude is slightly smaller. In order to verify that the potential gradient still does not obey an ambipolar relation, a calculation similar to that performed for Figs. 9 and 10 was performed at  $Q = 2\text{ sccm}$ ,  $B = 340\text{ G}$ , and  $P_{RF} = 100\text{ W}$  with the upstream endplate floating. The required electron temperature to satisfy a Boltzmann relation is  $kT_e = 11.7 \pm 0.8\text{ eV}$ , whereas the temperature measured with the double probe at  $z = 50\text{ cm}$  for the same conditions is  $kT_e = 7.6 \pm 0.5\text{ eV}$ , indicating that the expansion does not follow an ambipolar relation.

When the upstream endplate is grounded, there is an additional electron loss from the upstream region. There are two ways for the plasma to compensate for these extra losses. First, the time-averaged plasma potential upstream could increase to equalize the overall particle fluxes from the plasma. If the upstream time-averaged plasma potential increased enough alone to compensate for the extra electron losses, there would be no net current to the upstream plate and the acceleration due to the downstream potential gradient would be current-free, and the global net electron and ion losses would be equal. On the other hand, it is possible to support a net current flow through the upstream endplate, which would act to equalize overall electron and ion losses globally in the system. In reality, both an increase of the upstream plasma potential of  $\approx 20\text{ V}$  and a net positive current flowing from ground into the endplate (or a net negative (electron) current flowing from the plasma to the endplate)

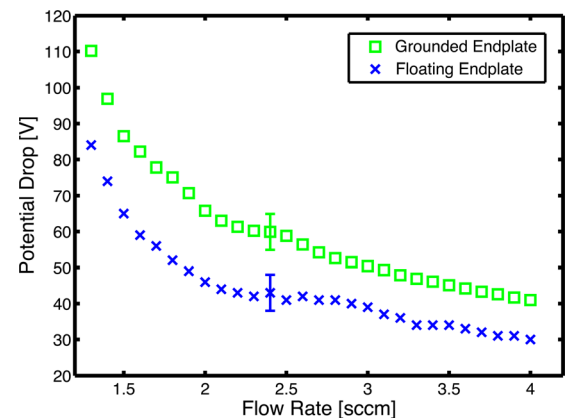


FIG. 11. Potential drop  $\Delta V$  vs argon flow rate for a grounded (green squares) and floating (blue  $\times$ s) for  $P_{RF} = 100\text{ W}$ ,  $B = 340\text{ G}$ . The potential drop is calculated from the difference between the RPA-measured time-averaged plasma potentials (ion potential energies) at  $z = 50\text{ cm}$  and  $z = 80\text{ cm}$ .

are observed. The (negative) electron current flows into the upstream endplate, through ground and back into the plasma through the downstream chamber. There cannot be an overall time-averaged net current flow out of or into the plasma or infinite charging of the plasma would occur. When the upstream endplate is isolated from ground (floating), there can be no net current to or from the plate in steady state. Since the upstream endplate's potential is not held at any particular value, it can charge with respect to the plasma such that the net ion and electron currents to the plate are zero in steady state. Most importantly, the potential gradient between the source and expansion chambers cannot be described by ambipolar plasma expansion alone, when the endplate is either grounded or floating, and is a result of the self-bias effect.

## VI. CONCLUSION

Previous measurements on the MadHeX system have revealed large potential differences (up to  $\Delta V = 165$  V at  $P_{RF} = 500$  W in the capacitive mode), evolving over several hundred Debye lengths, between the upstream, insulating source region and the downstream, grounded expansion chamber. New measurements using a swept emissive probe show the presence of significant fluctuations of the plasma potential ( $V_{p-p} \gtrsim 140$  V,  $V_{p-p}/\bar{V}_p \approx 150\%$ ) on the RF timescale when the source is operating in the capacitive (E) mode. In the inductive (H) mode, the magnitude of the fluctuations as well as the potential difference between the upstream and downstream regions decreases. The increased potential gradient and accompanying ion energy associated with the capacitive (E) mode are the result of a self-bias effect due to rapid fluctuations of the plasma potential. The more mobile electrons can easily respond to time-varying gradients in the plasma potential on the RF timescale, while the massive ions cannot and only respond to the effective or time-averaged value. Initially, plasma electrons are able to flow from the upstream region to the downstream region more readily than the ions, leading to an imbalance in total flux and charging of the plasma in the upstream region. However, the fluctuations of the plasma potential allow more electrons to escape the upstream region initially and the upstream time-averaged plasma potential increases beyond that of a DC sheath ( $\approx 5$  kTe/e) to enforce flux balance, known as the self-bias effect. The plasma ions are accelerated beyond that expected by ambipolar plasma expansion in response to the gradient in the time-averaged plasma potential. Rapid fluctuations of the plasma potential result in a time-dependent axial electron flux that acts to "neutralize" the accelerated ion population, resulting in a zero net time-averaged current through the acceleration region when an insulating upstream boundary condition is enforced. The effect of the upstream boundary condition was also explored, with a self-biasing observed both with the upstream end plate grounded and floating.

## ACKNOWLEDGMENTS

We thank Professor Wong of UCLA for fabrication of the 2-grid RPA and Professor Hershkovitz and Chi-Shung

Yip for assistance in fabrication of the emissive probe and tantalum probes. Research supported by AFOSR Grant No. FA9550-09-1-0357 and in part by AFOSR Grant No. FA9550-10-1-0396.

- <sup>1</sup>X. Sun, A. M. Keesee, C. Biloiu, E. E. Scime, A. Meige, C. Charles, and R. W. Boswell, "Observations of ion-beam formation in a current-free double layer," *Phys. Rev. Lett.* **95**(2), 025004 (2005).
- <sup>2</sup>C. Charles and R. Boswell, "Current free double layer formation in a high-density helicon discharge," *Appl. Phys. Lett.* **82**(9), 1356–1358 (2003).
- <sup>3</sup>C. Charles and R. W. Boswell, "Laboratory evidence of a supersonic ion beam generated by a current-free "helicon" double-layer," *Phys. Plasmas* **11**(4), 1706–1714 (2004).
- <sup>4</sup>J. Prager, R. Winglee, T. Ziemba, B. R. Roberson, and G. Quetin, "Ion energy characteristics downstream of a high power helicon," *Plasma Sources Sci. Technol.* **17**(2), 025003 (2008).
- <sup>5</sup>C. Charles and R. W. Boswell, "Time development of a current-free double-layer," *Phys. Plasmas* **11**(8), 3808–3812 (2004).
- <sup>6</sup>H. S. Byhring, C. Charles, A. Fredriksen, and R. W. Boswell, "Double layer in an expanding plasma: Simultaneous upstream and downstream measurements," *Phys. Plasmas* **15**(10), 102113 (2008).
- <sup>7</sup>V. F. Virko, Y. V. Virko, V. M. Slobodyan, and K. P. Shamrai, "The effect of magnetic configuration on ion acceleration from a compact helicon source with permanent magnets," *Plasma Sources Sci. Technol.* **19**(1), 015004 (2010).
- <sup>8</sup>Fredriksen, L. N. Mishra, and H. S. Byhring, "The effects of downstream magnetic field on current-free double layers and beam formation in the Njord helicon plasma device," *Plasma Sources Sci. Technol.* **19**(3), 034009 (2010).
- <sup>9</sup>E. E. Scime, I. A. Biloiu, J. J. Carr, S. C. Thakur, M. Galante, A. Hansen, S. Houshmandyar, A. M. Keesee, D. McCarren, S. Sears, C. Biloiu, and X. Sun, "Time-resolved measurements of double layer evolution in expanding plasma," *Phys. Plasmas* **17**(5), 055701 (2010).
- <sup>10</sup>S. A. Cohen, N. S. Siefert, S. Stange, R. F. Boivin, E. E. Scime, and F. M. Levinton, "Ion acceleration in plasmas emerging from a helicon-heated magnetic-mirror device," *Phys. Plasmas* **10**(6), 2593–2598 (2003).
- <sup>11</sup>N. Plihon, P. Chabert, and C. S. Corr, "Experimental investigation of double layers in expanding plasmas," *Phys. Plasmas* **14**(1), 013506 (2007).
- <sup>12</sup>C. S. Corr, J. Zanger, R. W. Boswell, and C. Charles, "Ion beam formation in a low-pressure geometrically expanding argon plasma," *Appl. Phys. Lett.* **91**, 241501 (2007).
- <sup>13</sup>C. S. Corr, R. W. Boswell, C. Charles, and J. Zanger, "Spatial evolution of an ion beam created by a geometrically expanding low-pressure argon plasma," *Appl. Phys. Lett.* **92**(22), 221508 (2008).
- <sup>14</sup>T. Lafleur, C. Charles, and R. W. Boswell, "Detailed plasma potential measurements in a radio-frequency expanding plasma obtained from various electrostatic probes," *Phys. Plasmas* **16**(4), 044510 (2009).
- <sup>15</sup>B. W. Longmier, E. A. B. III, M. D. Carter, L. D. Cassady, W. J. Chancery, F. R. C. Diaz, T. W. Glover, N. Hershkovitz, A. V. Ilin, G. E. McCaskill, C. S. Olsen, and J. P. Squire, "Ambipolar ion acceleration in an expanding magnetic nozzle," *Plasma Sources Sci. Technol.* **20**(1), 015007 (2011).
- <sup>16</sup>A. Dunaevsky, Y. Raitses, and N. J. Fisch, "Plasma acceleration from radio-frequency discharge in dielectric capillary," *Appl. Phys. Lett.* **88**(25), 251502 (2006).
- <sup>17</sup>C. Charles, "Plasmas for spacecraft propulsion," *J. Phys. D* **42**(16), 163001 (2009).
- <sup>18</sup>M. Lieberman and A. Lichtenberg, *Principles of Plasma Discharges and Materials Processing*, 2nd ed. (John Wiley and Sons, 2005).
- <sup>19</sup>P. Chabert and N. Braithwaite, *Physics of Radio-Frequency Plasmas* (Cambridge University Press, 2011).
- <sup>20</sup>Y. Raizer, M. Schnieder, and N. Yatsenko, *Radio-Frequency Capacitive Discharges* (CRC Press, 1995).
- <sup>21</sup>M. Wiebold, Y.-T. Sung, and J. E. Scharer, "Experimental observation of ion beams in the Madison Helicon eXperiment," *Phys. Plasmas* **18**(6), 063501 (2011).
- <sup>22</sup>J. R. Smith, N. Hershkovitz, and P. Coakley, "Inflection-point method of interpreting emissive probe characteristics," *Rev. Sci. Instrum.* **50**, 210–218 (1979).
- <sup>23</sup>J. P. Sheehan, Y. Raitses, N. Hershkovitz, and N. Fisch, "A comparison of inflection point and floating point emissive probe techniques for electric potential measurements in a Hall thruster plasma," in *APS Meeting Abstracts* (Nov. 2010), pp. 9015P–+.

- <sup>24</sup>T. Lho, N. Hershkowitz, and G.-H. Kim, "Effect of harmonic rf fields on the emissive probe characteristics," *Rev. Sci. Instrum.* **71**, 403–405 (2000).
- <sup>25</sup>T. Lho, N. Hershkowitz, G. H. Kim, W. Steer, and J. Miller, "Asymmetric plasma potential fluctuation in an inductive plasma source," *Plasma Sources Sci. Technol.* **9**(1), 5 (2000).
- <sup>26</sup>V. A. Godyak and V. I. Demidov, "Probe measurements of electron-energy distributions in plasmas: What can we measure and how can we achieve reliable results?" *J. Phys. D* **44**(23), 233001 (2011).
- <sup>27</sup>A. E. Wendt, "Passive external radio frequency filter for Langmuir probes," *Rev. Sci. Instrum.* **72**(7), 2926–2930 (2001).
- <sup>28</sup>L. Oksuz, F. Soberon, and A. R. Ellingboe, "Analysis of uncompensated Langmuir probe characteristics in radio-frequency discharges revisited," *J. Appl. Phys.* **99**(1), 013304 (2006).
- <sup>29</sup>A. Perry, G. Conway, R. Boswell, and H. Persing, "Modulated plasma potentials and cross field diffusion in a helicon plasma," *Phys. Plasmas* **9**(7), 3171–3177 (2002).
- <sup>30</sup>A. R. Ellingboe and R. W. Boswell, "Capacitive, inductive and helicon-wave modes of operation of a helicon plasma source," *Phys. Plasmas* **3**(7), 2797–2804 (1996).
- <sup>31</sup>S. M. Tysk, C. M. Denning, J. E. Scharer, and K. Akhtar, "Optical, wave measurements, and modeling of helicon plasmas for a wide range of magnetic fields," *Phys. Plasmas* **11**(3), 878–887 (2004).
- <sup>32</sup>C. M. Denning, M. Wiebold, and J. E. Scharer, "Observations of neutral depletion and plasma acceleration in a flowing high-power argon helicon plasma," *Phys. Plasmas* **15**(7), 072115 (2008).
- <sup>33</sup>M. D. West, C. Charles, and R. W. Boswell, "High density mode in xenon produced by a helicon double layer thruster," *J. Phys. D* **42**(24), 245201 (2009).